Ambient Pressure, Low-Temperature Synthesis and Characterization of Colloidal InN Nanocrystals

Ambient pressure, low-temperature synthesis and characterization of colloidal InN nanocrystals

Jennifer C. Hsieh,[a] Dong Soo Yun,[a] Evelyn Hu[b] and Angela M. Belcher*[ac]

Received 26th October 2009, Accepted 20th November 2009
First published as an Advance Article on the web 15th January 2010
DOI: 10.1039/b922196d

Highly soluble, non-aggregated colloidal wurtzite InN nanocrystals were obtained through an ambient pressure, low-temperature method followed by post-synthesis treatment with nitric acid.

Group III nitrides have attracted much attention for their optical and electronic properties, such as a wide range of direct band gaps and high electron mobility.[1] Of the three nitrides—AlN, GaN, and InN—InN has been the least studied, but recent results have shown strong potential for a variety of applications: its small effective mass and large intervalley energy separation promise high electron mobility for high-frequency devices;[2] its direct band gap and possibility for alloying with other III-nitride materials hold promise for broad-spectrum solar cell[3] devices. Exploring the possibilities for InN has provided much motivation for understanding its intrinsic materials properties, especially in light of the recently settled debate about its band gap. Amended from the previously accepted value of 1.9 eV, it is now widely accepted that the true band gap lies around 0.65–0.7 eV.[4,5] InN still remains a material with poor thermal stability and without suitable lattice-matched substrates for epitaxial growth. Therefore, one approach for studying the material is to eliminate the need for a substrate and synthesize InN as free-standing nanopowders. The formation of nanocrystalline InN makes possible the heterogeneous integration of InN with other materials and device structures, and allows for integration with the biological regime.[6] In addition, it is of interest to understand how defining characteristics, such as polarization, are manifested at the nanoscale. While several groups have grown InN nanoparticles through solvothermal autoclave methods,[7,8] ammonolysis,[9] thermal decomposition of indium–urea complexes,[10,11] or solid-state metathesis reactions,[12] the results were typically large agglomerations of nanocrystalline InN with no reports of high-yield colloidal solubility in organic or aqueous solvents.

Many groups have reported the formation of indium metal as a byproduct of InN nanoparticle synthesis.[12–14] Wells and Janik were unsuccessful using $InBr_3$ and Li_3N as precursors,[14] influencing other researchers, such as Xiao *et al.*[8] and Wu *et al.*[7] to specifically avoid $InBr_3$ in solvothermal methods. They cited $InBr_3$'s weaker covalent bond, as compared to In_2S_3 and InI_3, as a low barrier to indium metal formation, despite mild success in solid-state metathesis reactions.[12] In our work, we opted to re-examine the pyrolysis of $In(NH_2)_3$ from $InBr_3$ and $NaNH_2$ because these precursors are commercially available, relatively inexpensive, and easily handled. We found that not only could the metal in the resulting mixed metal–nitride product be preferentially removed, but it was also critical in making high-yield colloidal InN nanoparticles.

In the present work, we report a synthesis process for single-phase wurtzite InN nanocrystals using a previously dismissed simple halide salt precursor, $InBr_3$. In addition, our method functions at both low-temperature (250 °C) and ambient pressure, which reduces many of the complications implicit to autoclave, solvothermal-based procedures. Post-reaction processing of the resulting mixed metal–nitride aggregates released the nitride nanoparticles from the large aggregations. Subsequently, when combined with an appropriate surfactant, these individual nanoparticles were easily dispersed in organic solvents, forming brown transparent solution. Our colloidal nanoparticles are substrate independent, amenable to large-area deposition methods, and allow for optical measurements of non-aggregated InN nanoparticles.

In a typical synthesis, 1 mmol of $InBr_3$ was combined with 3 mmol of $NaNH_2$ in 10 mL of hexadecane under a nitrogen atmosphere. For the duration of the reaction, ammonia gas flowed through the flask, creating an oxygen-free atmosphere and allowing the synthesis to remain at ambient pressure. The solution was stirred briskly and heated to 180 °C for 10 min, then ramped to 250 °C over 3 h. The solution was held at 250 °C for 10 h and cooled to room temperature over 5 h. Post-synthesis processing began with separating hexadecane from the resulting black solid by centrifugation followed by a wash with hexane. The black solid was then rinsed with hot methanol to remove NaBr salt. The dried powder was subsequently sonicated with 3.4% nitric acid for 2 min, which oxidized the metal. The sample was then washed with ethanol, and immediately immersed in excess oleylamine. After sonicating the product in oleylamine for 5 min, excess oleylamine was removed by centrifugation with ethanol, and the particles were suspended in toluene. Once in solution, the particles remained stable and did not precipitate over several months.

Powder X-ray diffraction (XRD) was conducted on a Rigaku X-Ray Diffractometer with Cu-Kα radiation operating at 300 mA and 50 kV to determine both the resulting crystal structure of the InN and to verify the removal of indium metal. Fig. 1 depicts the diffraction spectrum of a typical sample before nitric acid treatment in post-reaction processing (a) and the diffraction spectrum of an aliquot of the same sample after nitric acid treatment (b). The two sets of three peaks at 2θ = 28–34° and 50–64° correspond to wurtzite phase InN with lattice parameters $a = 3.547 \pm 0.002$ Å, $c = 5.759 \pm 0.016$ Å and grain sizes of 6.6 ± 2.0 nm. The lattice values are close to previously published values for InN nanopowders, $a = 3.552$ Å, $c = 5.716$ Å.[8] Removal of the metal was confirmed by the disappearance

[a]*Department of Materials Science and Engineering, Massachusetts Institute of Technology, 77 Massachusetts Avenue, Cambridge, MA, 02139, USA. E-mail: belcher@mit.edu; Tel: +1 617 3242800*
[b]*Department of Engineering and Applied Sciences, Harvard University, 29 Oxford Street, Cambridge, MA, 02138, USA*
[c]*Department of Biological Engineering, Massachusetts Institute of Technology, 77 Massachusetts Avenue, Cambridge, MA, 02139, USA*

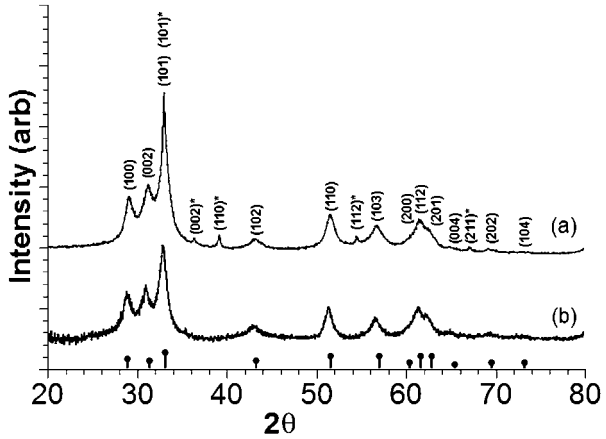

Fig. 1 Normalized XRD data of InN nanoparticle synthesis products before (a) and after (b) post-reaction nitric acid treatment. Nitric acid treatment removes indium metal peaks at $2\theta = 36°$ and 39°. Reference positions of wurtzite InN peaks lie along the bottom axis of the plot. Starred indices correspond to indium metal.

of peaks at $2\theta = 36°$ and 39° and a change in the intensity ratios of peaks $2\theta = 29° : 33°$ from 1 : 3.2 to 1 : 2.1. Rietveld analysis showed no evidence of preferred orientation.

The chemical states of the nanoparticles before and after nitric acid treatment were further examined by X-ray photoelectron spectroscopy (XPS). XPS data were collected with a Kratos Axis 165 using monochromatic Al-Kα of photon energy 1486.6 eV over a 400 × 700 μm^2 area and a maximum depth of 10 nm. The data were calibrated to the C 1s peak (284.8 eV). Examination of the In $3d_{5/2}$ and In $3d_{3/2}$ peaks of the powder before nitric acid treatment shows two separate chemical species. In Fig. 2, the peaks at 444.8 eV and 452.2 eV correspond to In–N bonds[15–17] while the peaks at 443.8 eV and 451.3 eV correspond to indium metal.[18] As shown in Fig. 2a, the deconvoluted peaks are a very good fit with the observed data. The calculated peaks for Fig. 2b reveal a slight asymmetry in the observed data, but no additional peak could be reasonably extracted from the

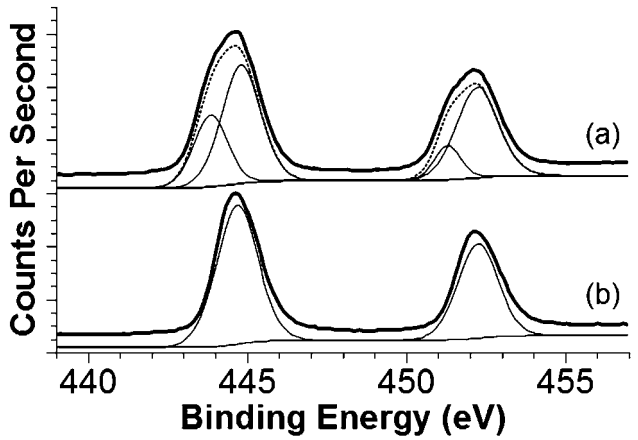

Fig. 2 XPS data of the In $3d_{5/2}$ and In $3d_{3/2}$ before (a) and after (b) post-reaction nitric acid treatment. Two distinct chemical states corresponding to indium metal and indium–nitride can be seen before treatment (a). The metallic indium chemical species is no longer detectable after treatment (b). Calculated fits (thin lines) have been offset from the data (thick lines) for clarity. The dashed line is the sum of the calculated fits.

data. Calculating the chemical state ratios from the peak areas gives an average nitride : metal atomic ratio of 79.7 : 20.2. Atomic ratios of In : N were measured to be 1.2 : 1 after acid treatment, using commercially available InN powder (Aldrich, 99.9% metals basis) as a reference standard. Our relative peak areas are similar to two previous reports, though it is unknown whether those reports used a standard to calibrate their quantitative results.[7,16]

High resolution transmission electron microscope (HRTEM) images were taken on a JEOL 2010F TEM at 200 kV. Fig. 3 shows the distribution and crystallinity of the resulting InN nanoparticles. Before the nitric acid treatment, the large agglomerations were similar to the morphologies of previously reported nanopowders.[8,13] The morphology after the acid treatment is shown in Fig. 3a; the aggregations separated into many smaller, individual, irregularly shaped InN nanocrystals, which were easily solubilized in toluene with the addition of oleylamine. Although the particles were irregularly shaped, the average particle "diameter" was approximated by averaging the particle areas as seen under HRTEM. From the highly polydisperse particles seen in Fig. 3a, our average particle size was 6.2 ± 2.0 nm, in close agreement with the XRD FWHM estimations. Diffraction patterns obtained from fast Fourier transformation (FFT) of high resolution images (Fig. 3b and c), confirmed that these InN single crystals have the ⟨0001⟩ zone axis for wurtzite InN with $P6_3mc$ space group. The nearest three spots in the diffraction patterns with [0001] zone axis can be indexed to the $(10\bar{1}0)$, $(01\bar{1}0)$ and $(\bar{1}100)$ planes. According to the lattice fringes of the InN nanocrystals, the lattice spacing between two planes is ~0.307 nm, corresponding to the distance of two {100} planes (JCPDS01-088-2362). Theoretically, the angle between the nearest spots should be 60° and the distance between origin point and spots should be the same in the single crystal

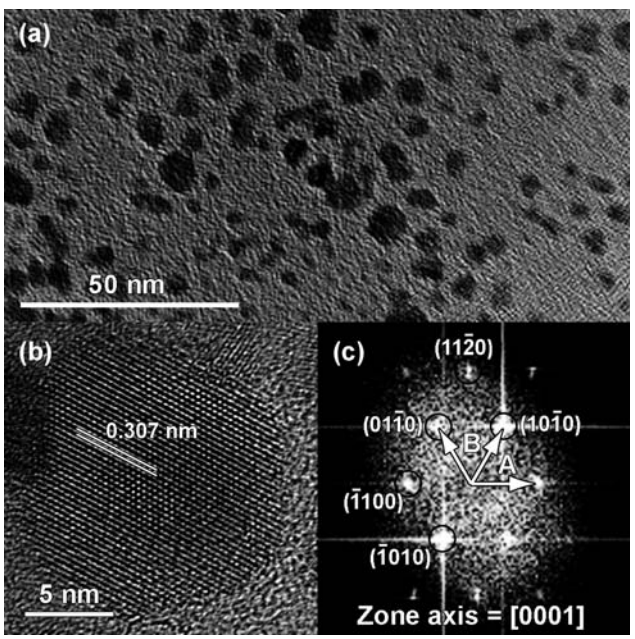

Fig. 3 TEM images of the synthesis product after nitric acid treatment. (a) Low magnification image showing well-dispersed and non-aggregated nanoparticles. (b) High resolution image depicting single-crystalline nature of nanoparticles. Lattice spacing corresponds to the distance between two {100} planes. (c) Diffraction pattern obtained by fast Fourier transform (FFT) of high resolution TEM image (b).

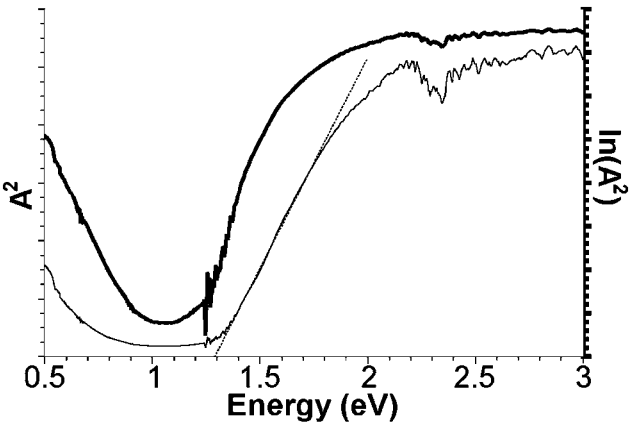

Fig. 4 Optical absorption at room temperature shows band gap of 1.29 eV. The log of the absorbance squared shows an Urbach band tail region from 0.5–0.9 eV. Using 0.5 eV as a rough estimate of the maximum Moss–Burstein shift, the actual band gap may be ~0.8 eV.

with [0001] zone axis. As seen in the diffraction pattern, both interplanar angles measured among three spots are ~60° and the ratio of B to A is ~1, consistent with theoretical values of [0001] zone axis.

Absorption measurements on sample powders were taken on a Cary 5E spectrophotometer with a praying mantis diffuse reflection accessory and referenced to KBr. IR photoluminescence measurements were conducted in toluene at room temperature and at 77 K on a Fluorolog equipped with argon laser (488 nm) excitation. Absorption data indicate an extrapolated band gap value of 1.29 eV (Fig. 4). This value is larger than 0.7–0.9 eV but lower than the earlier quoted value of 1.9 eV.[19–21] It has already been observed that InN has a strong propensity for n-type conductance,[22,23] and absorption measurements of the band gap are influenced by the Moss–Burstein effect.[5,24–26] This in turn may be related to the polarity of the InN surface, and recent studies that have indicated In presence on the surface, regardless of polarity.[27] We have not assessed the polarity of our samples, nor have we determined the electron concentration of our InN nanocrystals, but a rough estimate of the maximum value of the Moss–Burstein shift from our room temperature absorption data suggests that the actual band gap may be ~0.8 eV. More detailed, temperature-dependent measurements of the absorption data would give a better estimate of the actual band gap. No luminescence was observed between 550 nm and 1600 nm at room temperature or at 77 K. We also did not observe the commonly seen fluorescence at 650 nm (1.9 eV), which is attributed to oxygen defects.[28] Despite the high levels of crystallinity observed under TEM, nitrogen deficiencies or a high density of surface traps in our samples may be obstructing band edge emission in this work.

In summary, we have successfully synthesized colloidal wurtzite InN nanocrystals with an average diameter of 6.2 ± 2.0 nm utilizing $InBr_3$ and $NaNH_2$ in a low-temperature, ambient pressure, liquid-phase method. XRD, XPS, and TEM data showed that using a post-synthesis acid treatment, we were able to leverage what was considered an undesirable byproduct, indium metal, into a critical sacrificial component for the formation of highly soluble oleylamine coated nanocrystals in toluene. This method may be applicable for the synthesis of other nanoparticle materials that have low decomposition temperatures or high levels of extraneous byproducts. Absorption data indicate the InN nanopowder synthesized herein has a band gap value of ~0.8 eV, which may be related to the nitrogen deficient nature of the material, and further studies are under way to better understand the optical and electronic structure of this material.

Acknowledgements

The authors acknowledge the support of the NSF Graduate Fellowship and National Cancer Institute CCNE Project Grant.

Notes and references

1 B. Monemar, *J. Mater. Sci.: Mater. Electron.*, 1999, **10**, 227–254.
2 S. K. O'Leary, B. E. Foutz, M. S. Shur and L. F. Eastman, *Appl. Phys. Lett.*, 2006, **88**, 3.
3 A. Yamamoto, M. Tsujino, M. Ohkubo and A. Hashimoto, *7th International Photovoltaic Science and Engineering Conference (PVSEC-7)*, Elsevier Science Bv, Nagoya, Japan, 1993, pp. 53–60.
4 T. Matsuoka, H. Okamoto, M. Nakao, H. Harima and E. Kurimoto, *Appl. Phys. Lett.*, 2002, **81**, 1246–1248.
5 V. Y. Davydov and A. A. Klochikhin, in *Indium Nitride and Related Alloys*, ed. C. F. M. T. D. Veal and W. J. Schaff, Taylor and Francis Group, LLC, Baton Rouge, FL, 2009, pp. 181–241.
6 X. Michalet, F. F. Pinaud, L. A. Bentolila, J. M. Tsay, S. Doose, J. J. Li, G. Sundaresan, A. M. Wu, S. S. Gambhir and S. Weiss, *Science*, 2005, **307**, 538–544.
7 C. Z. Wu, T. W. Li, L. Y. Lei, S. Q. Hu, Y. Liu and Y. Xie, *New J. Chem.*, 2005, **29**, 1610–1615.
8 J. P. Xiao, Y. Xie, R. Tang and W. Luo, *Inorg. Chem.*, 2003, **42**, 107–111.
9 B. Schwenzer, C. Meier, O. Masala, R. Seshadri, S. P. DenBaars and U. K. Mishra, *J. Mater. Chem.*, 2005, **15**, 1891–1895.
10 K. Sardar, M. Dan, B. Schwenzer and C. N. R. Rao, *J. Mater. Chem.*, 2005, **15**, 2175–2177.
11 S. Podsiadlo, *Thermochim. Acta*, 1995, **256**, 375–380.
12 R. W. Cumberland, R. G. Blair, C. H. Wallace, T. K. Reynolds and R. B. Kaner, *J. Phys. Chem. B*, 2001, **105**, 11922–11927.
13 Y. J. Bai, Z. G. Liu, X. G. Xu, D. L. Cui, X. P. Hao, X. Feng and Q. L. Wang, *J. Cryst. Growth*, 2002, **241**, 189–192.
14 R. L. Wells and J. F. Janik, *Eur. J. Solid State Inorg. Chem.*, 1996, **33**, 1079–1090.
15 W. D. Yang, P. N. Wang, F. M. Li and K. W. Cheah, *Nanotechnology*, 2002, **13**, 65–68.
16 F. X. Wang, C. S. Xue, H. Z. Zhuang, X. K. Zhang, Y. J. Ai, L. Sun, Z. Z. Yang and H. Li, *Physica E (Amsterdam)*, 2008, **40**, 664–667.
17 Y. J. Xiong, Y. Xie, Z. Q. Li, X. O. Li and R. Zhang, *New J. Chem.*, 2004, **28**, 214–217.
18 Z. W. Li, X. J. Tao, Y. M. Cheng, Z. S. Wu, Z. J. Zhang and H. X. Dang, *Mater. Sci. Eng., A*, 2005, **407**, 7–10.
19 K. Osamura, S. Naka and Y. Murakami, *J. Appl. Phys.*, 1975, **46**, 3432–3437.
20 N. Puychevrier and M. Menoret, *Thin Solid Films*, 1976, **36**, 141–145.
21 T. L. Tansley and C. P. Foley, *J. Appl. Phys.*, 1986, **59**, 3241–3244.
22 P. D. C. King, T. D. Veal and C. F. McConville, in *Indium Nitrideand Related Alloys*, ed. C. F. M. T. D. Veal and W. J. Schaff, Taylor and Francis Group, LLC, Baton Rouge, FL, 2009, pp. 121–137.
23 J. Wu and W. Walukiewicz, *Superlattices Microstruct.*, 2003, **34**, 63–75.
24 B. Monemar, P. P. Paskov and A. Kasic, *Superlattices Microstruct.*, 2005, **38**, 38–56.
25 V. Y. Davydov and A. A. Klochikhin, *Semiconductors*, 2004, **38**, 861–898.
26 K. S. A. Butcher, H. Hirshy, R. M. Perks, M. Wintrebert-Fouquet and P. P. T. Chen, *Phys. Status Solidi A*, 2005, **203**, 66–74.
27 T. D. Veal, P. D. C. King, P. H. Jefferson, L. F. J. Piper, C. F. McConville, H. Lu, W. J. Schaff, P. A. Anderson, S. M. Durbin, D. Muto, H. Naoi and Y. Nanishi, *Phys. Rev. B: Condens. Matter*, 2007, **76**, 8.
28 A. G. Bhuiyan, A. Hashimoto and A. Yamamoto, *J. Appl. Phys.*, 2003, **94**, 2779–2808.